Cambridge Centre for Computational Chemical Engineering

University of Cambridge

Department of Chemical Engineering

Preprint ISSN 1473 – 4273

Modelling soot particle size distribution: Dynamics of pressure regimes

Jasdeep Singh, Robert Patterson, Michael Balthasar, Markus Kraft [1], Wolfgang Wagner[2]

submitted: 27th September 2004

[1] Department of Chemical Engineering University of Cambridge Pembroke Street Cambridge CB2 3RA United Kingdom E-Mail:mk306@cam.ac.uk

[2] Weierstrass Institute for Applied Analysis and Stochastic Mohrenstraße 39 D-10117 Berlin Germany E-Mail: wagner@wias-berlin.de

Preprint No. 25

c4e

Key words and phrases. Soot, Particle size distribution, Laminar premixed flames, Stochastic processes, Majorant kernels, Pressure regimes.

Edited by
Cambridge Centre for Computational Chemical Engineering
Department of Chemical Engineering
University of Cambridge
Cambridge CB2 3RA
United Kingdom.

Fax: + 44 (0)1223 334796
E-Mail: c4e@cheng.cam.ac.uk
World Wide Web: http://www.cheng.cam.ac.uk/c4e/

Abstract

In this paper we present a stochastic algorithm designed for all relevant pressures to model the formation, growth and oxidation of soot particles. The stochastic method is used to solve the population balance equation that describes the various processes of soot formation, e.g., nucleation, coagulation, and surface reactions. We introduce a new generalized majorant kernel to exploit the method of fictitious jumps reducing the computational expense for the direct simulation algorithm. The implementation of the stochastic algorithm is validated against LSODE (Livermore Solver for Ordinary Differential Equation). We investigate laminar premixed flames to obtain the temporal evolution of the soot particle size distribution. The moments of these distributions are compared to the experimental measurements and existing numerical methods. A good agreement is observed. The effect of change in the C/O molar ratio on soot particle size distributions is discussed in the light of surface reactions contributing to the soot growth and oxidation. Also, it is demonstrated that the soot particle size distributions conform to the recent experimental observations, which link the nature of the distribution, i.e. bimodal, uni-modal, to the peak temperature of the flame. A further study was done to show the importance of considering the different pressure regimes. A detailed description of the algorithm is given to facilitate its implementation by the reader.

Contents

1 Introduction

Soot formation, growth and oxidation has been extensively researched for many years [5, 24]. The latest soot models include elaborate gas phase reaction kinetics [2, 32] and well defined processes leading to the formation and oxidation of soot [14] along with fast numerical techniques [12] to solve the models. More recently, the community has advanced to the modelling of soot aggregates and also soot formation at high pressures [21]. Alongside the modelers, experimental groups have used scanning mobility particle sizer (SMPS) [35] and noninvasive techniques such as the small-angle neutron scattering [33] and small-angle X-ray scattering [19] to improve the spatial and size resolution of the measurements to 2–3 nm.

Although progress has been made in the understanding of the essential chemistry and physics of soot formation, many questions persist and debate continues regarding the details of soot phenomenology. Physical questions such as the smallest size of soot particles, the soot inception model, the number of active sites on the surface of the soot particle for reaction with the surrounding gaseous species [11, 29] as well as the computational questions such as the approximations used by the existing numerical techniques are the issues that have motivated this paper.

In order to isolate these different issues, one is interested in investigating the spatial and temporal evolution of the soot particle size distribution in simple systems, e.g. laminar premixed flames [15]. Various numerical techniques have been developed to predict the properties of the soot population. Of these numerical techniques, the Method of Moments (MoM) [13] and sectional techniques (Discrete sectional Method and Galerkin Method) [3, 16, 30] have dominated the literature. The Method of Moments, which is a fast technique, solves for the first few moments of the soot particle size distribution. In contrast, sectional techniques provide some resolution of the size distribution at the cost of additional computational expense. In recent years the stochastic approach [17, 28], which is pertinent to this paper, has shown promising results in overcoming the approximations used by the previously mentioned techniques. The main feature of this approach is that it converges to the exact solution of the population balance equation [8]. This technique has been improved to reduce computational time through the concept of the 'majorant kernel' [6, 7]. Furthermore, the modelling of higher dimensional distributions is relatively straightforward and the size and the age of soot particles are known explicitly. Previously, this approach has been used for the first time to simulate soot formation and oxidation in sub-atmospheric laminar premixed flames [4]. Here, all the processes of soot formation and oxidation are treated probabilistically and performed exactly.

The **purpose of this paper** is to extend the stochastic method, previously applied to sub atmospheric pressure flames, to higher pressure laminar premixed flames. A detailed algorithm is put forward, along with a new majorant kernel to reduce the computational time, which serves as a reference for the reader to implement. Using this algorithm, the temporal evolution of the soot particle size distributions for atmospheric and higher pressure laminar premixed flames are obtained and compared

qualitatively with recent experimental observations in [35, 36].

The paper is organized in the following manner. In section 2 the soot model and the kernels describing the interaction of soot particles in the different pressure regimes are elaborated upon. In section 3 an algorithm solving the dynamics of the size distribution of the soot particles using the concept of the 'majorant kernel' is explained. In section 4 the implementation of the stochastic approach is validated against a differential equation solver and the results of simulated flames covering relevant pressure regimes are presented. These are compared with the solutions obtained from the MoM and experimental measurements along with analysis of the regimes the soot particles are in. The paper closes with a conclusion section which includes pointers for future work.

2 Model

The formation and oxidation of soot is a result of many different chemical and physical processes. These include reactions between the surface of the soot particle and the surrounding gaseous species; coagulation, aggregation and inception. In this paper we use a simplified model [2]. The model has three types of processes:

1. The smallest soot particle is **incepted** upon the collision of two gaseous pyrene molecules and no other type of inception occurs;
2. **Coagulation** is modelled as the coalescence of two soot particles;
3. There are four **surface reactions** with the surrounding gaseous species:
   (a) condensation of Pyrene, which adds 16 carbon atoms to the soot particle
   (b) surface growth by Acetylene through the Hydrogen Abstraction Carbon Addition (HACA) mechanism, which adds 2 carbon atoms to the soot particle
   (c) oxidation by O_2, which removes two carbon atoms from the soot particle, and
   (d) oxidation by OH, which removes a single carbon atom from the soot particle.

The differential equation describing the temporal evolution of the soot population according to the model is the following:

$$\begin{aligned}\frac{\partial}{\partial t}c(t,i) &= \underbrace{I c^{in}\,(i)}_{\text{Inception}} + \underbrace{\sum_{\ell=1}^{4}\left[\beta^{\ell}_{i-\delta\ell}\;\delta(i)\;c(t,i-\delta\ell) - \beta^{\ell}_{i}\;c(t,i)\right]}_{\text{Surface reactions}} \\ &\quad \underbrace{+\frac{1}{2}\sum_{j=1}^{i-1}\beta_{i-j,j}\;c(t,i-j)\;c(t,j) - \sum_{j=1}^{\infty}\beta_{i,j}\;c(t,i)\;c(t,j)}_{\text{Coagulation}}, \qquad (1)\end{aligned}$$

and

$$\delta\ell = \begin{cases} 16 & \text{for } \ell = 1: \text{ Condensation,} \\ 2 & \text{for } \ell = 2: \text{ Acetylene addition,} \\ -2 & \text{for } \ell = 3: \text{ } O_2 \text{ oxidation,} \\ -1 & \text{for } \ell = 4: \text{ OH oxidation,} \end{cases} \qquad (2)$$

$$c^{in}(i) = \begin{cases} 1 & \text{for } i = 32, \\ 0 & \text{otherwise,} \end{cases} \qquad (3)$$

$$\delta(i) = \begin{cases} 0 & \text{if an oxidation process results in } i < 32, \\ 1 & \text{for rest of the cases,} \end{cases} \qquad (4)$$

with the initial condition

$$c(0,i) = c_0(i) = 0 \quad \text{for all } i,$$

where $c(t,i)$ is the concentration of soot particles composed of i carbon atoms at a time t. β^{ℓ}_{i} is the rate of the ℓ^{th} surface reaction for a particle of size i. $\beta_{i,j}$ is the coagulation kernel and takes a different form in each pressure regime, which is elaborated in the section 2.1.

2.1 Coagulation kernel in different pressure regimes

The kernels are determined by the physics involved in the interaction of pairs of particles. In general, the main drivers of particle transport are Brownian motion, gravitational settling and turbulence, the latter two being not important in the context of laminar premixed flames. A classification on the basis of the Knudsen number ($Kn = 2\lambda/d$, where λ is the gas mean free path and d the soot particle diameter) is done in order to define kernels for different pressure regimes. Figure 1 illustrates the categorization of regimes based on the Knudsen number. It indicates the operating regime for a soot particle given the pressure of the flame, the temperature of the surrounding gas, and the size of the soot particle. For example, a particle of diameter 30 nm at a temperature of 1400 K in a 1 bar flame will be in the free

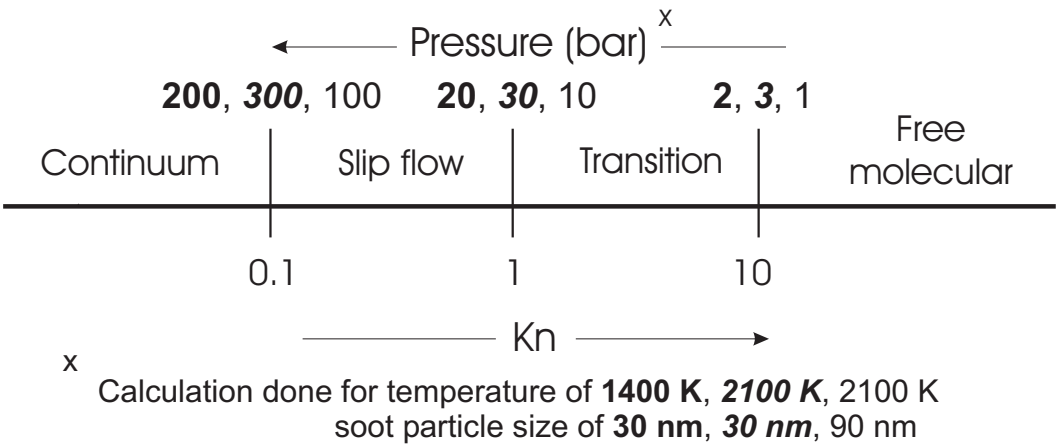

Figure 1: *Categorization of pressure regimes based on the Knudsen number.*

molecular regime, whereas a particle of diameter 90 nm at a temperature of 2100 K in a 10 bar flame will be in the transition regime. The values of the temperature and soot particle diameters for the figure have been chosen to represent conditions in different parts of flames.

2.1.1 Continuum regime ($Kn \leq 0.1$)

This regime is applicable when the size of the particle is large relative to the mean free path of the gas molecules and hence the fluid acts as a continuum, with the movement of the molecules given by diffusion theory. The derivation of the coagulation kernel assumes a Stokes' law drag coefficient and takes the form:

$$\beta_{i,j}^{c} = K_0 \ (i^{-1/3} + j^{-1/3})(i^{1/3} + j^{1/3}), \tag{5}$$

where

$$K_0 = \frac{2k_B T}{3\mu},$$

k_B is the Boltzmann constant, T is the temperature, and μ is the viscosity of the fluid.

2.1.2 Slip flow regime ($0.1 < Kn \leq 1$)

The diffusion theory model is extended to $Kn = 1$ by modifying Stokes' law with a factor C, which is a function of Kn. As in [21], we take the factor C to be:

$$C_i = 1 + 1.257 \times Kn_i,$$

where,

$$Kn_i = 2\lambda/d_i,$$

and d_i is the diameter of a soot particle containing i carbon atoms.

Thus, we obtain

$$\beta_{i,j}^{sf} = K_0 \left(\frac{C_i}{i^{1/3}} + \frac{C_j}{j^{1/3}} \right) (i^{1/3} + j^{1/3}).$$

After the substitutions, we get

$$\beta_{i,j}^{sf} = K_0 \left(i^{1/3} + j^{1/3}\right) \left[\left(i^{-1/3} + j^{-1/3}\right) + \left(i^{-2/3} + j^{-2/3}\right) \mathbf{U} \right], \tag{6}$$

where

$$\mathbf{U}(T, P) = 1.257 \times Kn_1 (T, P).$$

It should be noted that in the limit of low Knudsen numbers the correction factor $C \to 1$, thus approaching the continuum regime kernel.

2.1.3 Free molecular regime ($Kn > 10$)

This regime applies when the particles are small relative to the mean free path. This occurs when the pressure of the flame is atmospheric or lower. The collision rate is calculated through statistical mechanics by averaging over the velocity distribution in the fluid. The rate is augmented by including van der Waals forces and a correction for sticking probability of the soot particles [20]. This leads to the following form of the kernel.

$$\beta_{i,j}^{fm} = A \left(i^{-1} + j^{-1}\right)^{1/2} \left(i^{1/3} + j^{1/3}\right)^2, \tag{7}$$

where

$$A = 2.2 \left(\frac{3m_1}{4\pi\rho_s} \right)^{1/6} \left(\frac{6k_B T}{\rho_s} \right)^{1/2},$$

m_1 is the mass of a single carbon atom, and ρ_s is the density of the soot particle. These values are given in the appendix 4.

2.1.4 Transition regime ($1 < Kn \leq 10$)

The Boltzmann equation and diffusion theory model, applicable in the free molecular and continuum regimes respectively, cannot be extended into the transition regime, which lies in between. Therefore, Pratsinis [26] developed an approximate kernel valid for the transition regime, which was motivated by the Fuchs kernel [21].

$$\beta_{i,j}^{t} = \beta_{i,j}^{sf} \left[1 + \frac{\beta_{i,j}^{sf}}{\beta_{i,j}^{fm}} \right]^{-1}. \tag{8}$$

The kernel, which is twice the harmonic mean of the slip flow and the free molecular kernels, is a complicated function of the soot particle size.

3 Stochastic Particle Method

This section will illustrate a stochastic approach to solve Eq. 1 for the model described and presents a direct simulation algorithm. Equation 1 is a more general form of the basic discrete Smoluchowski coagulation equation, which has been solved analytically and stochastically for simple kernels [1, 28, 31]. The equation has also been numerically solved for complicated kernels with the Method of Moments [12] and stochastically [18, 4, 29] using the concept of majorant kernels [7]. The majorant kernel is a tool for reducing the computational expense of the direct simulation algorithm (DSA) and an extension of it is used in the following section for the transition regime.

3.1 Majorant kernel for the transition regime

The majorant kernel, $\widehat{\beta}_{i,j}$, used to evaluate R_{coag} (see appendix B) should have the following properties:

1. It must be greater than or equal to the coagulation kernel $\beta_{i,j}$ for all i, j;
2. Calculating the total coagulation rate R_{coag} should be fast;
3. It should have a high efficiency, i.e. $\beta_{i,j}/\widehat{\beta}_{i,j}$ as close to 1 as possible so that R_{coag} is as small as possible.

The majorant kernel for the free molecular regime, $\widehat{\beta}^{fm}_{i,j}$, was developed by Goodson and Kraft [18] and was seen to reduce the complexity of simulating the coagulation process from $\mathcal{O}(N^2)$ to $\mathcal{O}(N)$. The kernel is given by:

$$\widehat{\beta}^{fm}_{i,j} = 1.4178 \times A\ (i^{-\frac{1}{2}} + j^{-\frac{1}{2}})(i^{\frac{2}{3}} + j^{\frac{2}{3}}). \tag{9}$$

Achieving all the three goals above is not easy in the transition regime, so we introduce a majorant rate which is a slight generalization of the majorant kernel concept.

First we derive a majorant for Eq. 8 that meets criteria 1 and 3. We note that no majorant is required for the slip flow regime and we have already referred to a majorant for the free molecular regime so, following the harmonic mean idea, we define:

$$\frac{1}{\overline{\beta}^{\,t}_{i,j}} := \frac{1}{\widehat{\beta}^{fm}_{i,j}} + \frac{1}{\beta^{sf}_{i,j}},$$

and since $\widehat{\beta}^{fm}_{i,j} \geq \beta^{fm}_{i,j}$ we have:

$$\frac{1}{\overline{\beta}^{\,t}_{i,j}} \leq \frac{1}{\beta^{fm}_{i,j}} + \frac{1}{\beta^{sf}_{i,j}} = \frac{1}{\beta^{\,t}_{i,j}},$$

which implies

$$\overline{\beta}_{i,j}^{\,t} \geq \beta_{i,j}^{\,t}. \tag{10}$$

However, $\overline{\beta}^{\,t}$ is not suitable for use as a majorant because it does not satisfy criteria 2. We proceed to a slightly larger majorant kernel with the definition:

$$\tilde{\beta}_{i,j}^{\,t} := \min\left(\widehat{\beta}_{i,j}^{fm}, \beta_{i,j}^{sf}\right) \geq \overline{\beta}_{i,j}^{\,t} \geq \beta_{i,j}^{\,t}.$$

Evaluating R_{coag} using $\tilde{\beta}^{\,t}$ is still slow - $\mathcal{O}(N^2)$ since every pair of particles has to be considered. Defining $\tilde{R}_{coag}^{\,t}$ as the value of R_{coag} resulting from setting $\beta = \tilde{\beta}^{\,t}$ in the definition of R_{coag} in appendix B and $\widehat{R}_{coag}^{fm}$ analogously we have a majorant rate $\widehat{R}_{coag}^{\,t}$ for the transition regime given by (note that there is no $\widehat{\beta}^{\,t}$):

$$\widehat{R}_{coag}^{\,t} := \min\left(\widehat{R}_{coag}^{fm}, R_{coag}^{sf}\right) \geq \tilde{R}_{coag}^{t} \geq R_{coag}^{t}.$$

If $\widehat{R}_{coag}^{fm} \leq R_{coag}^{sf}$ the time step proceeds using $\widehat{\beta}^{fm}$ as a majorant kernel, otherwise β^{sf} is used.

In section 4.4 we record the proportion of fictitious coagulation events resulting from the use of this majorant for various flames, the figure never exceeds 40%.

3.2 The Algorithm

The stochastic algorithm for solving the Smoluchowski equation follows:

1. Generate the initial state, for all the flames we simulate in this paper this initial condition is 0 particles.

2. Wait an exponentially distributed time step τ, with parameter

$$\begin{aligned} R(p) &= R_{\text{coag}}(p) + R_{\text{pin}}(p) + R_{\text{cond}}(p) + R_{\text{sg}}(p) + R_{\text{O}_2\ \text{ox}}(p) + R_{\text{OH ox}}(p), \\ \tau &= -\frac{\ln(y)}{R(p)}, \quad y \text{ is a uniformly distributed random number between 0 and 1.} \end{aligned}$$

   where R_i for each regime are defined in appendix B and R_{coag} is calculated based on the majorant kernels.

3. With probability

$$\frac{R_\omega(p)}{R(p)},$$

   go to step ω, where $\omega = 4$ is Particle inception, $\omega = 5$ is Surface growth by C_2H_2, $\omega = 6$ is Oxidation by O_2, $\omega = 7$ is Oxidation by OH, $\omega = 8$ is Coagulation, and $\omega = 9$ is Condensation. ω may be generated using the standard inverse transform method, see for example algorithm 'DI' in § 3.2.4 of [9].

4. **Perform inception**, i.e.

   (a) Add a particle of size 32 to the ensemble and go to step 2.

5. **Perform surface growth by** C_2H_2, i.e.

   (a) Select a particle of size i weighting each particle by its surface area.

   (b) Remove the particle of size i, add a particle of size $i+2$ to the ensemble.

   (c) Go to step 2.

6. **Perform oxidation by** O_2, i.e.

   (a) Select a particle of size i weighting each particle by its surface area.

   (b) Remove the particle of size i and

      i. add a particle of size $i-2$, if $i \neq 32$ or $i \neq 33$.

      ii. If $i = 32$ or $i = 33$, then the model treats the particle as oxidized back to the gas phase and it is not replaced in the ensemble.

   (c) Go to step 2.

7. **Perform oxidation by OH**, i.e.

   (a) Select a particle of size i weighting each particle by its surface area.

   (b) Remove the particle of size i and

      i. add a particle of size $i-1$, if $i \neq 32$.

      ii. If $i = 32$, then the model treats the particle as oxidized back to the gas phase and it is not replaced in the ensemble.

   (c) Go to step 2.

8. **Perform coagulation** , i.e.

   If operating in the transition regime go to step 8f, else go to step 8a

   (a) With probability

   $$Y_i / \sum_{i=1}^{4} Y_i$$

   go to step 8b for $i = 1$, step 8c for $i = 2$, step 8d for $i = 3$, and step 8e for $i = 4$. Y_i are defined for each regime in appendix B.

   (b) The particles are selected by observing the terms in the expression Y_1:

      i. Select a particle of size i uniformly from the ensemble;

      ii. Select a particle of size j uniformly from the ensemble for the continuum and the slip flow regime and weighted by mass to the power one-sixth for the free molecular regime;

      iii. If $i = j$, then go to step 8b, otherwise go to step 8g.

(c) The particles are selected by observing the terms in the expression Y_2:

i. Select a particle of size i weighted by mass to the power one-third for the continuum and the slip flow regime and by mass to the power one-sixth for the free molecular regime;

ii. Select a particle of size i weighted by mass to the power minus one-third for the continuum and the slip flow regime and by mass to the power minus one-half for the free molecular regime;

iii. If $i = j$, then go to step 8c, otherwise go to step 8g.

(d) The particles are selected by observing the terms in the expression Y_3:

i. Select a particle of size i uniformly from the ensemble for the slip flow regime;

ii. Select a particle of size j weighted by mass to the power minus one-third for the slip flow regime;

iii. If $i = j$, then go to step 8d, otherwise go to step 8g.

(e) The particles are selected by observing the terms in the expression Y_4:

i. Select a particle of size i weighted by mass to the power minus one-third for the slip flow regime;

ii. Select a particle of size j weighted by mass to the power minus two-third for the slip flow regime;

iii. If $i = j$, then go to step 8e, otherwise go to step 8g.

(f) **Procedure for the transition regime**.

Evaluate the rate of coagulation, R_{coag}, for the free-molecular (R^{fm}_{coag}) and the slip flow (R^{sf}_{coag}) regimes. These are defined in appendix B.

i. If $R^{fm}_{coag} \geq R^{sf}_{coag}$, then go to step 8a with Y_1, Y_2 from the free-molecular regime and $\widehat{\beta}^{\,t} = \widehat{\beta}^{fm}$ else

ii. go to step 8a with Y_1, Y_2, Y_3, Y_4 from the slip flow regime and $\widehat{\beta}^{\,t} = \widehat{\beta}^{sf}$

(g) Perform the (possibly fictitious) coagulation

i. With probability

$$1 - \frac{\beta_{i,j}}{\widehat{\beta}_{i,j}}$$

calculated using the kernels from the active regime (note that $\widehat{\beta}^{sf} \equiv \beta^{sf}$) the event is fictitious so do not alter the particle ensemble and go to step 8(g)iii else

ii. remove the particles of size i and j, add a particle of size $i + j$

iii. go to step 2

9. **Perform a condensation step**, i.e.

If operating in the transition regime go to step 9e, otherwise go to step 9a

(a) With probability

$$Z_i / \sum_{i=1}^{3} Z_i$$

go to step 9b for $i = 1$, step 9c for $i = 2$, step 9d for $i = 3$. Z_i is defined for each regime in Appendix B.

(b) Select a particle of size i uniformly from the ensemble and go to step 9f.

(c) Select a particle of size i weighted by mass to the power one-third and go to step 9f.

(d) Select a particle of size i weighted by the surface area of the particle for the free molecular regime and by mass to the power minus one-third for the slip flow and the continuum regimes. Go to step 9f.

(e) **Procedure for the transition regime**.
Evaluate the rate of condensation-R_{cond} for the free molecular (R^{fm}_{cond}) and the slip flow (R^{sf}_{cond}) regimes. These are defined in Appendix B.

i. If $R^{fm}_{cond} \geq R^{sf}_{cond}$, then go to step 9a with Z_1, Z_2, Z_3 from the free-molecular regime and $\widehat{\beta}^{t,cond} = \beta^{fm,cond}$ else

ii. Go to step 9a with Z_1, Z_2, Z_3 from the slip flow regime and $\widehat{\beta}^{t,cond} = \beta^{sf,cond}$

(f) Perform the (possibly fictitious) condensation event

i. If the original regime was anything except transition go to step 9(f)iii else

ii. with probability

$$1 - \frac{\beta_i^{t,cond}}{\widehat{\beta}_i^{t,cond}}$$

the event is fictitious so do not alter the particle ensemble and go to step 9(f)iv else

iii. remove the particle of size i, add a particle of size $i + 16$

iv. go to step 2

The above algorithm along with the results obtained from PREMIX [23] are used to solve for the soot particle size distribution. PREMIX, a one dimensional premixed laminar flame code, provides the concentration of various gaseous species and temperature as a function of time or distance from the burner. It uses an elaborate reaction mechanism [32] and has been modified to account for soot growth [25].

The authors would be happy to provide a FORTRAN 90/95 implementation of this algorithm on request.

4 Numerical Results

In this section we test the implementation of the algorithm and discuss results obtained from simulating premixed flames with varying properties, such as the operating pressure and the C/O molar ratio.

4.1 Validity of the algorithm

Before presenting results for real flames we show data for some specially constructed test cases. These cases were chosen such that high quality numerical solutions to Eq. 1 were readily obtainable using LSODE [27] and to test all the features of our code. We did this by devising a set of chemical and physical conditions for each pressure regime that led to each of the four surface reactions described in Section 2 having rates of a similar order of magnitude (unlike most physical cases where they vary by many orders).

An important acceleration of LSODE was achieved by redefining the $\delta\ell$ of Eq. 2 as follows:

$$\delta\ell = \begin{cases} 16 & \text{for } \ell = 1: \text{ Condensation,} \\ 4 & \text{for } \ell = 2: \text{ Acetylene addition,} \\ -8 & \text{for } \ell = 3: \text{ } O_2 \text{ oxidation,} \\ -4 & \text{for } \ell = 4: \text{ OH oxidation,} \end{cases}$$

so we only had to solve Eq. 1 for $i = 32, 36, 40...$ one quarter of the number of size classes needed for the physically realistic cases. LSODE can only solve Eq. 1 for a finite number of size classes. We ensured that the number of size classes used enabled LSODE to handle the largest particles that we observed in our stochastic simulations and which led to negligible number densities for the largest size classes. We found our results to be stable under variations of this parameter.

LSODE uses an adaptive stepping method to advance the solution over time. We set the error control to restrict the estimated relative error introduced in each time step to 1×10^{-6} for every component of the solution. This was intended to ensure that the relative error in all components of the final solution was small, altering this relative tolerance by a factor of 10 was not found to affect our results.

We used a range of settings to collect the stochastic simulation results shown here, as for LSODE we experimented with the parameter values to check that the results were independent of the values we used. All the results shown are averaged over at least 20 repetitions of the simulations with the number of computational particles over 32768 except in the initial phases. We achieved 95% confidence intervals of less than $\pm 2\%$ for the first few size classes. Figure 2 shows the solution to Eq. 1 obtained in the test cases as described above. As can be seen in the figure, we ran the simulations for long enough to develop a range of particle sizes. The figure provides a clear illustration of the convergence results given in [8], which say that the data obtained by DSA should converge to a solution of Eq. 1 as the number of

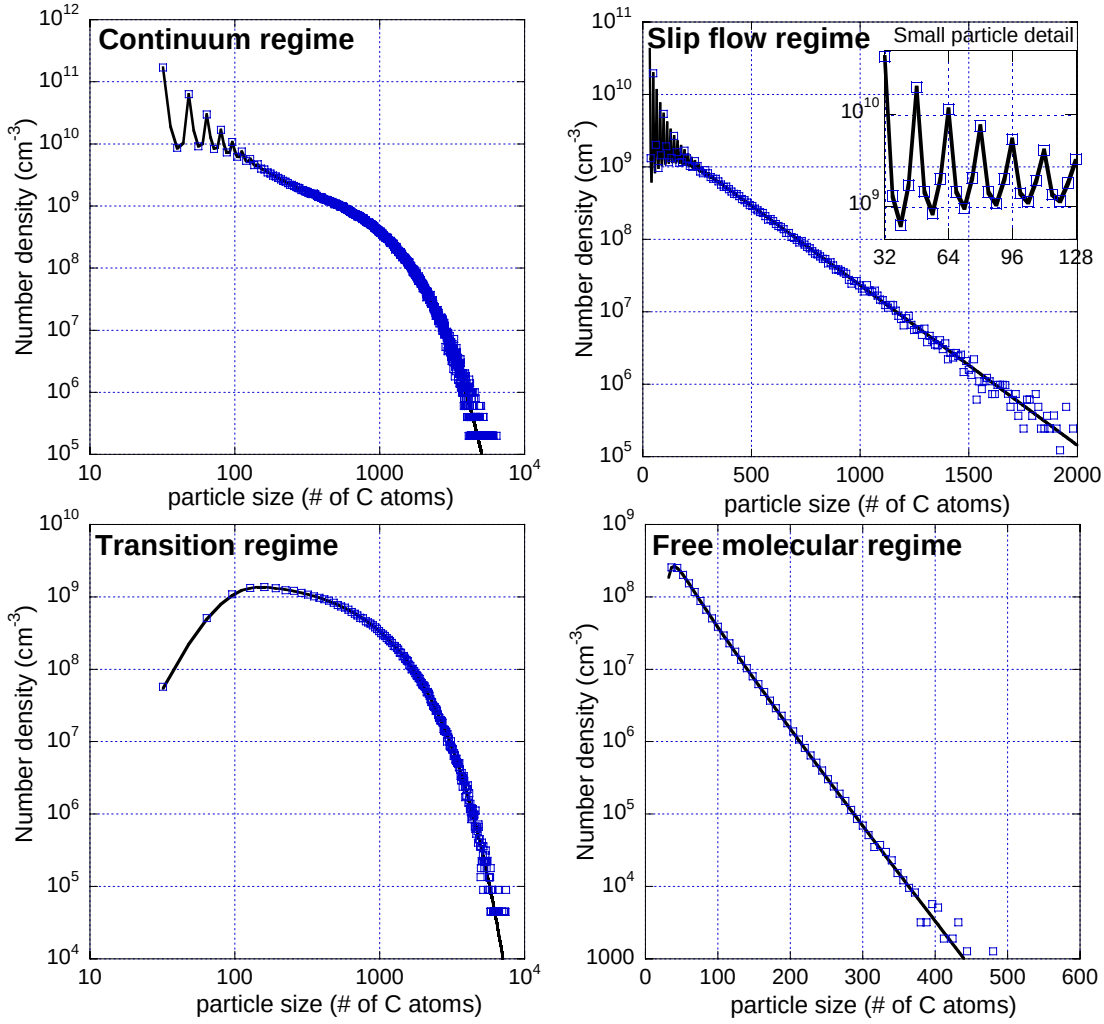

Figure 2: *Comparison of the soot particle size distribution between the LSODE (—) and the Direct Simulation Algorithm (□)*

computational particles used tends to infinity. These results give us confidence that the results we now present in Sec. 4.2 are accurate solutions of Eq. 1 for the relevant input data.

4.2 Simulation of laminar premixed flames

Four laminar premixed flames (Table 1), with varying properties and from different experimental groups [36, 34, 22], were selected. We chose these flames to cover a range of pressures, C/O ratios, and maximum temperatures.

Table 1: *Properties of the laminar premixed flames*

Flame	Mole fraction			C/O ratio	T_{max} (K)	Velocity (cm/s)	Pressure (bar)
	C_2H_4	O_2	N_2				
HW1.64	0.242	0.379	0.379	0.64	1790	8.0	1
XSF1.78	0.14	0.18	0.68	0.78	2104	4.0	1
JW10.60	0.112	0.1865	0.7015	0.60	2015	6.0	10
JW10.68	0.125	0.184	0.691	0.68	1880	6.0	10

The flames, two each from 1 and 10 bar with C/O ratio ranging from 0.64 – 0.78 and maximum temperature from 1790 K – 2104 K were simulated. Figure 3 shows the

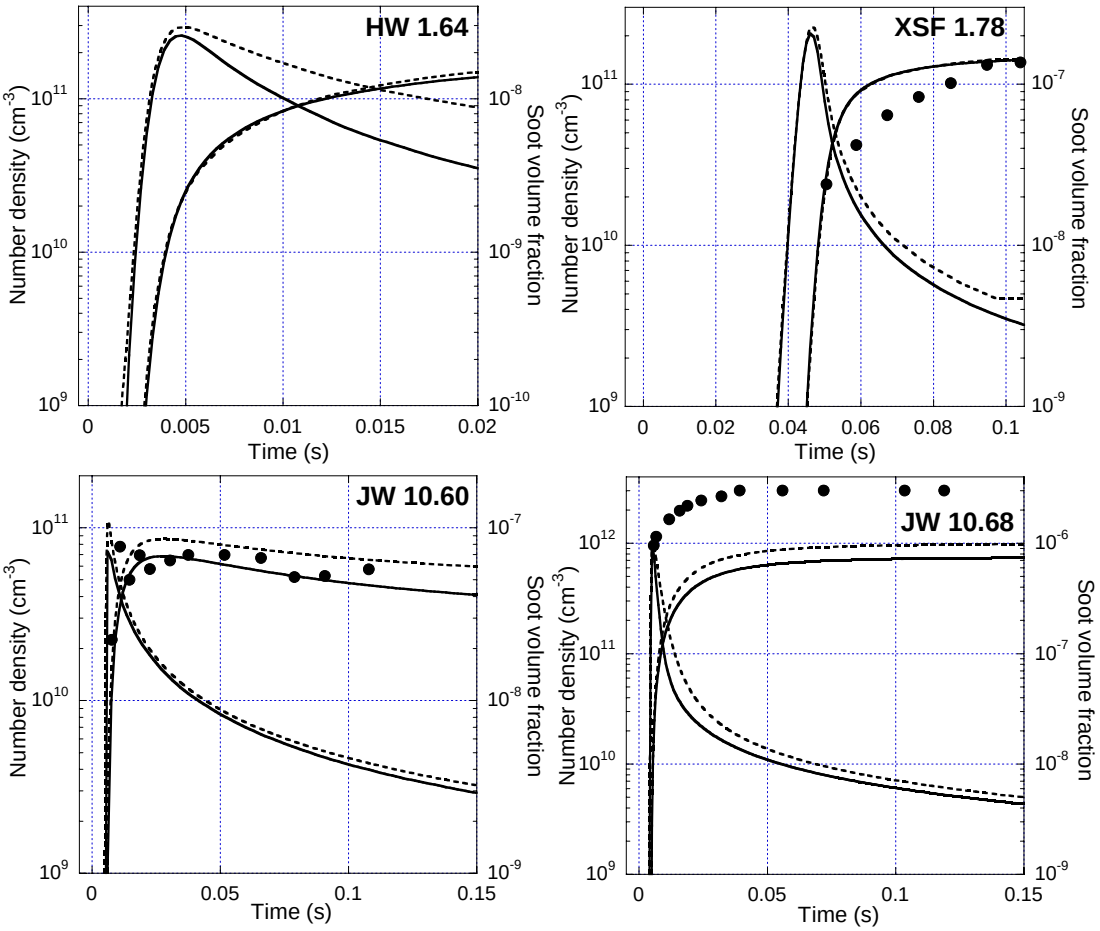

Figure 3: *Comparison of the Number density and Soot volume fraction between the DSA (—), Method of Moments (- - -), and Experimental measurements (•)*

comparison of the number density and soot volume fraction between the DSA, MoM, and experimental measurements [36, 34, 22] for the laminar premixed flames. Only the normalized soot particle size distribution was available for the flame HW 1.64 and thus the soot volume fraction could not be plotted in Fig. 3. A good agreement is observed between the DSA and MoM. In this work, MoM is used as published in [2] and the code is available on the internet [10]. In this version two important

approximations are made, which account for the difference in the two numerical techniques:

1. Interpolation techniques are used to evaluate the coagulation term in the Eq. 1;
2. The oxidation simply causes a change in the mean particle mass without accounting for the possibility of very small particles being oxidized back into the gaseous phase.

This would explain why the MoM predicts higher particle number density than DSA for all the four flames, especially in the flame HW 1.64, where the bi-modal distribution means that small particles are present at all times and so have a greater effect.

The prediction of DSA for the soot volume fraction matches the experimental measurements for the flames XSF 1.78 and JW 10.60. However, the results for the flame JW 10.68, though matching in the trend, are off by a factor of 4. The difference between the measurements and numerical prediction is attributable to problems in modelling the number of active sites on the surface of soot particles that are available for reaction with the surrounding gaseous species. Here, the active sites on the surface of the soot particle are calculated by a fit developed [2] from the data available from 8 laminar premixed flames. This fit introduces an error. For the flames where the surface reactions are the dominant processes, such as the flame JW 10.68, the error gets magnified. This motivated us to study the relationship of soot particle age and active sites on the surface of the particle [29].

The stochastic method also gives a detailed information of properties associated with soot particles, e.g. size, surface area, and age. Figure 4 shows the size distributions of the soot particles at different times.

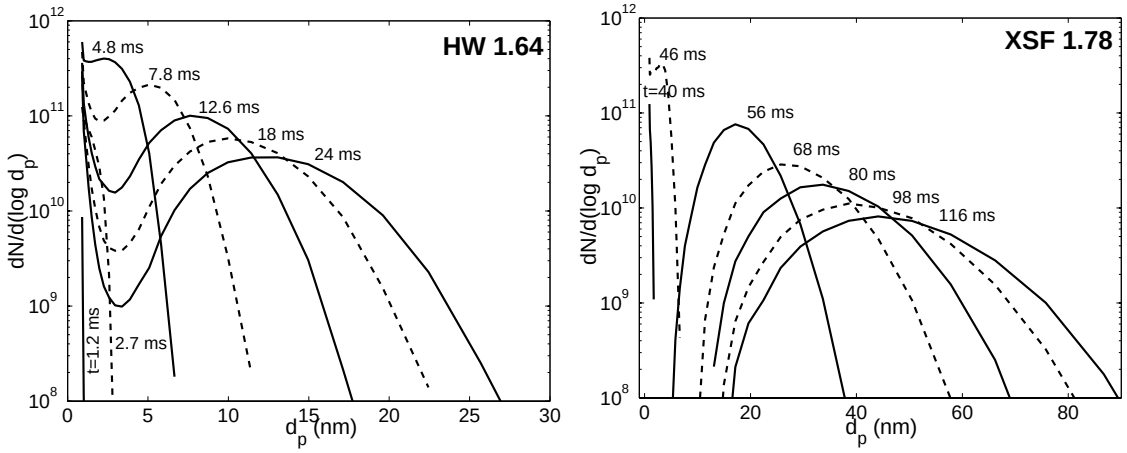

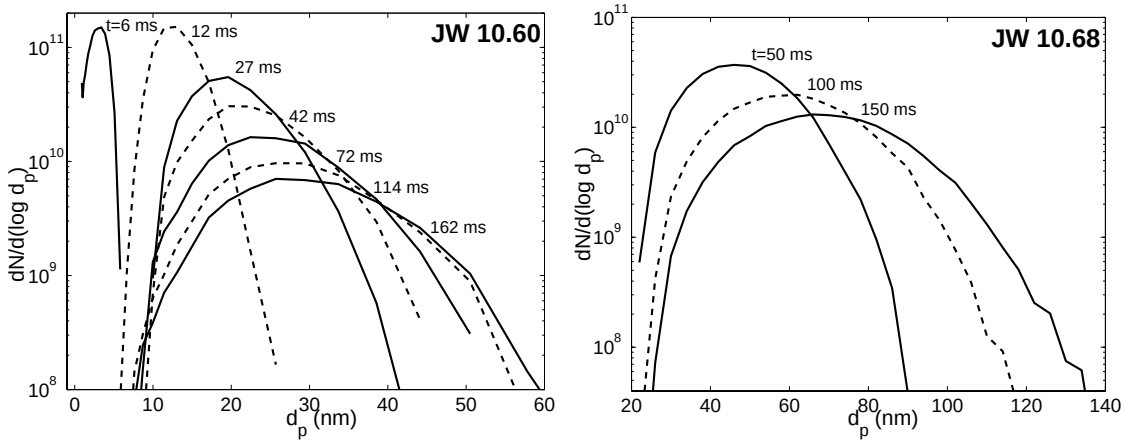

Figure 4: *Soot particle size distribution of the laminar premixed flames*

Both bi-modal and uni-modal distributions are observed. In [36] SMPS measurements have been carried out and the soot particle size distributions are linked to the maximum flame temperature. The authors suggested that for the temperature range of 1700 K–1850 K, the size distributions are bi-modal. The simulated soot particle size distribution of flame HW 1.64 agrees with this proposition.

Figure 4 also shows the effect of the C/O ratio at a constant pressure on the soot particle size distribution. It is observed that the maximum and mean size of the soot particle increases with the C/O ratio. The primary reason for this is the large relative increase in the rate of the C_2H_2 addition compared to the other surface reactions. In the flame JW 10.60, the size distribution alters very little at later times because the rate of OH oxidation compensates for the growth by C_2H_2 addition and Pyrene condensation. The shift in the distribution is thus a result of coagulation, which has a small rate. Whereas, in the flame JW 10.68, the C_2H_2 addition dominates the surface reaction processes and together with coagulation gives rise to the shift in the distribution towards the larger particles. The same reasoning holds true for the flames HW 1.64 and XSF 1.78.

4.3 Pressure regime study

A further study was done to observe the regimes the soot particles were in for various operating pressures in the flame. Knowing the regime of the particle in advance enables the selection of an efficient majorant kernel thus reducing the computational time. For this study, the chemical conditions were those of the flame JW 10.68. The pressure input to the stochastic soot model was varied from 1 to 100 bar without altering the flame chemistry predicted by PREMIX in the 10 bar case.

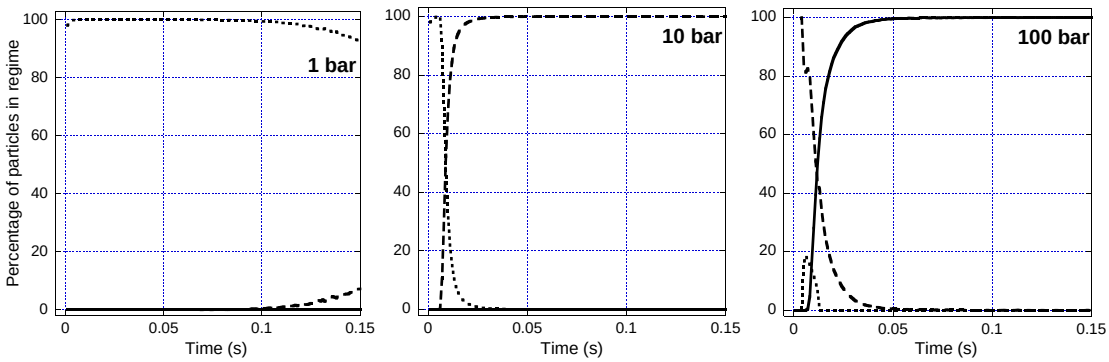

Figure 5: *Percentage of soot particles in the Free molecular regime (· · ·), Transition regime (- - -), and Slip flow regime (—) at 1, 10, 100 bar operating pressure of a flame*

Figure 5 illustrates the percentage of coagulation partners in different regimes for varying pressures in the flame. It is observed that these soot particles are dominantly in the free molecular regime for the 1 bar flame, transition regime for the 10 bar flame, and slip flow regime for the 100 bar flame. The study justifies the extension of stochastic algorithm to higher operating pressures of flames.

4.4 Performance

We observed the efficiency of the majorant kernel, which we define as the number of coagulation jumps performed divided by the number of times the coagulation event was selected. It was seen that the efficiency of the majorant kernel for the flame HW 1.64 was 0.87, flame XSF 1.78 was 0.80, and flame JW 10.60 was 0.61. These numbers depict a satisfactory performance of the majorant kernel. However, while simulating the four flames we observed that the simulation times were of the order of hours compared to minutes in [4]. The reasons for this were the following:

1. Particle doubling [28], a variance reduction technique, was used to obtain accurate soot particle size distributions for later times;

2. The rate of processes contributing to the soot formation and oxidation were higher by orders of magnitude than in [4]. This resulted in extremely short time steps and thus increased the computational time.

3. The number of stochastic particles representing the soot ensemble was higher than in [4].

All of the above reasons contributed to large simulation times for the flames. This issue was addressed by developing a new more efficient algorithm, which we used in [29] and which will be detailed in future publications.

5 Conclusions

This paper presents a stochastic method for solving the population balance equation describing the formation, growth, and oxidation of soot particles. It extends previous work by including coagulation mechanisms valid at higher pressures, such as the transition, slip flow, and continuum coagulation kernels. We introduced a new generalized majorant kernel to cover these higher pressure regimes. This enabled us to accelerate the simulations using the concept of fictitious jumps. The implementation of the stochastic algorithm was validated against LSODE. This extended stochastic algorithm was then applied to laminar premixed flames operating at pressures ranging from 1 bar - 10 bar to obtain the soot particle size distributions for different positions in these flames. The moments of these distributions were compared to the experimental measurements and the solutions obtained from the Method of Moments. The agreement between the numerical methods and experimental measurements was good.

The effect of change in the parameters such as the C/O ratio, the operating pressure, and the peak temperature of the flame were studied. It was observed that the mean and the maximum size of the soot particle increased with the C/O ratio with the surface growth by C_2H_2 addition playing an important role in it. We demonstrated the importance of considering the different pressure regimes by showing the extent to which they are used at higher pressures. Also, the nature of the soot size distribution (bi-modal or uni-modal) obtained from the simulations matched the recent experimental measurements. However, this needs to be investigated further as the experiments were limited to atmospheric pressure flames.

This work will facilitate investigation into the soot model as it implements the model exactly. The present work shall be augmented by accounting for effects due to a more detailed soot model and development of more efficient stochastic algorithms.

Acknowledgements

The support of Churchill College, Cambridge, is gratefully acknowledged. MB acknowledges the support of the Marie Curie program under the call FP6-2002-Mobility-5. and the Royal Society. WW acknowledges the EPSRC (Grant number GR/R85662/01) for the financial support.

A Summary of kernels

Table 2: *Summary of the kernels for processes in different regimes*

	Free molecular regime	Continuum regime
Coagulation	$A\left(i^{-1}+j^{-1}\right)^{\frac{1}{2}}\left(i^{\frac{1}{3}}+j^{\frac{1}{3}}\right)^{2}$	$K_0\left[2+(i/j)^{\frac{1}{3}}+(j/i)^{\frac{1}{3}}\right]$
Nucleation	$2.2\left(\frac{\pi k_B T}{m_c}\right)^{\frac{1}{2}} d_{PAH}^2$	$4K_0$
Condensation	$\left[C_1+C_2\ i^{\frac{1}{3}}+C_3\ i^{\frac{2}{3}}\right]$ $C_3=0.55\ \left(\frac{6m_c}{\pi\rho_s}\right)^{\frac{2}{3}}\sqrt{\frac{\pi k_B T}{2\ m_c}}$ $C_2=\sqrt{\frac{128}{3}}\ d_1\left(\frac{\pi\rho_s}{6m_c}\right)^{\frac{1}{3}} C_3$ $C_1=\sqrt{\frac{8}{3}}\ d_1\left(\frac{\pi\rho_s}{6m_c}\right)^{\frac{1}{3}} C_2$	$K_0\left[2+(i/16)^{\frac{1}{3}}+(16/i)^{\frac{1}{3}}\right]$
	Slip flow regime	Transition regime
Coagulation	$K_0\left(i^{\frac{1}{3}}+j^{\frac{1}{3}}\right)\times$ $\left[\left(i^{-\frac{1}{3}}+j^{-\frac{1}{3}}\right)+\mathbf{U}\left(i^{-\frac{2}{3}}+j^{-\frac{2}{3}}\right)\right]$	$\left[\left(\beta_{i,j}^{fm,coag}\right)^{-1}+\left(\beta_{i,j}^{sf,coag}\right)^{-1}\right]^{-1}$
Nucleation	$4K_0\left[1+\mathbf{U}\,(16)^{-\frac{1}{3}}\right]$	$\left[\left(\beta^{fm,nucl}\right)^{-1}+\left(\beta^{sf,nucl}\right)^{-1}\right]^{-1}$
Condensation	$K_0\left[\left(2+\frac{\mathbf{U}}{(16)^{\frac{1}{3}}}\right)+i^{-\frac{1}{3}}\left(\mathbf{U}+(16)^{\frac{1}{3}}\right)\right]$ $+K_0\left(\frac{i}{16}\right)^{\frac{1}{3}}\left(1+\frac{\mathbf{U}}{(16)^{\frac{1}{3}}}\right)$	$\left[\left(\beta_i^{fm,cond}\right)^{-1}+\left(\beta_i^{sf,cond}\right)^{-1}\right]^{-1}$

B Rate of processes

The rate of the processes, which are used to calculate the probability of the occurrence of the processes and the time step for the markovian process, are as follows:

$$
\begin{aligned}
\underline{\text{Particle Inception}}\,(\mathrm{R_{pin}}) \;:\; &= \frac{1}{2}\,\beta_{16,16}\,(C_{PAH}N_A)^2\,N \\
\underline{\text{Coagulation}}\,(\mathrm{R_{coag}}) \;:\; &= \frac{1}{2N}\left[\sum_{32\le i,j\le i_{max},j_{max}} (\beta_{i,j}N_iN_j) - \sum_{32\le i\le i_{max}} \beta_{i,i}N_i\right] \\
\text{Free molecular} \;&= \frac{A}{N}\left[\underbrace{(n-1)\sum_{i=32}^{i_{max}} N_i\; i^{\frac{1}{6}}}_{Y_1} + \underbrace{\left(\sum_{i=32}^{i_{max}} N_i\; i^{\frac{2}{3}}\sum_{i=32}^{i_{max}} N_i\; i^{-\frac{1}{2}} - \sum_{i=32}^{i_{max}} N_i\; i^{\frac{1}{6}}\right)}_{Y_2}\right] \\
\text{Continuum} \;&= \frac{K_0}{N}\left[\underbrace{n(n-1)}_{Y_1} + \underbrace{\sum_{i=32}^{i_{max}} N_i\; i^{\frac{1}{3}}\sum_{i=32}^{i_{max}} N_i\; i^{-\frac{1}{3}} - n}_{Y_2}\right] \\
\text{Slip flow} \;&= \frac{K_0}{N}\left[\underbrace{n(n-1)}_{Y_1} + \underbrace{\sum_{i=32}^{i_{max}} N_i\; i^{\frac{1}{3}}\sum_{i=32}^{i_{max}} N_i\; i^{-\frac{1}{3}} - n}_{Y_2}+\right. \\
&\qquad \left.\underbrace{\mathbf{U}(n-1)\sum_{i=32}^{i_{max}} N_i\; i^{-\frac{1}{3}}}_{Y_3} + \underbrace{\mathbf{U}\left(\sum_{i=32}^{i_{max}} N_i\; i^{\frac{1}{3}}\sum_{i=32}^{i_{max}} N_i\; i^{-\frac{2}{3}} - \sum_{i=32}^{i_{max}} N_i\; i^{-\frac{1}{3}}\right)}_{Y_4}\right]
\end{aligned}
$$

For the coagulation, $\beta_{i,j}$ is replaced by $\widehat{\beta}_{i,j}$ for the free molecular regime. The $\beta_{16,16}$ for the particle inception is taken from the Table 2. N, n, i_{max} are the normalization factor, total number of particles per cm^3 and maximum size of the soot particle respectively. Note the definition of the Y_i by means of the under-braces.

$$
\begin{aligned}
\underline{\text{Condensation}}\,(\mathrm{R_{cond}}) \;:\; &= C_{PAH}\; N_A \sum_{i=32}^{i_{max}} \beta_{i,16} N_i \\
\text{Free molecular} \;&= C_{PAH}\; N_A \left[\underbrace{C_1\; n}_{Z_1} + \underbrace{C_2 \sum_{i=32}^{i_{max}} N_i\; i^{\frac{1}{3}}}_{Z_2} + \underbrace{C_3 \sum_{i=32}^{i_{max}} N_i\; i^{\frac{2}{3}}}_{Z_3} \right] \\
\text{Continuum} \;&= C_{PAH}\; N_A\; K_0 \times \\
&\left[\underbrace{2n}_{Z_1} + \underbrace{(16)^{-\frac{1}{3}} \sum_{i=32}^{i_{max}} N_i\; i^{\frac{1}{3}}}_{Z_2} + \underbrace{(16)^{\frac{1}{3}} \sum_{i=32}^{i_{max}} N_i\; i^{-\frac{1}{3}}}_{Z_3} \right] \\
\text{Slip flow} \;&= C_{PAH}\; N_A\; K_0 \times \left[\underbrace{(16)^{-\frac{1}{3}} \left(1 + \frac{\mathbf{U}}{(16)^{\frac{1}{3}}} \right) \sum_{i=32}^{i_{max}} N_i\; i^{\frac{1}{3}}}_{Z_2} + \right. \\
&\left. \underbrace{\left(2 + \frac{\mathbf{U}}{16^{\frac{1}{3}}} \right) n}_{Z_1} + \underbrace{\left(\mathbf{U} + (16)^{\frac{1}{3}} \right) \sum_{i=32}^{i_{max}} N_i\; i^{-\frac{1}{3}}}_{Z_3} \right]
\end{aligned}
$$

Note the definition of the Z_i by means of the under-braces.

$$
\begin{aligned}
\underline{\text{Surface Growth by } \mathrm{C_2H_2}}\,(\mathrm{R_{sg}}) \;&:= fR_4 \times \text{Ratio fb} \times \text{eff sites} \times \sum_{i=32}^{i_{max}} N_i\; i^{\frac{2}{3}} \\
\underline{\text{Oxidation by } \mathrm{O_2}}\,(\mathrm{R_{O_2\ ox}}) \;&:= fR_5 \times \text{Ratio fb} \times \text{eff sites} \times \sum_{i=32}^{i_{max}} N_i\; i^{\frac{2}{3}} \\
\underline{\text{Oxidation by OH}}\,(\mathrm{R_{OH\ ox}}) \;&:= fR_6 \sqrt{\frac{\pi k_B T}{2 m_{OH}}} \left(\frac{6 m_c}{\pi \rho_s} \right)^{\frac{2}{3}} N_A \times \sum_{i=32}^{i_{max}} N_i\; i^{\frac{2}{3}}
\end{aligned}
$$

The constants for the surface reactions are defined in the table 3.

Table 3: *Surface reactions of soot particles with the gaseous species.*

$C_{soot}-H+\ H$	$\rightleftharpoons$	$C_{soot}*+\ H_2$	(fR_1, rR_1)
$C_{soot}-H+\ OH$	$\rightleftharpoons$	$C_{soot}*+\ H_2O$	(fR_2, rR_2)
$C_{soot}*+\ H$	$\rightarrow$	$C_{soot}-H$	(fR_3)
$C_{soot}*+\ C_2H_2$	$\rightarrow$	$C_{soot}-H+\ H$	(fR_4)
$C_{soot}*+\ O_2$	$\rightarrow$	products	(fR_5)
$C_{soot}-H+\ OH$	$\rightarrow$	products	(fR_6)

The rates of each reaction are as follows:

$$
\begin{aligned}
fR_1 &= 4.2 \times 10^{13}\ e^{-\left(\frac{13}{RT}\right)}\ C_H \\
rR_1 &= 3.9 \times 10^{12}\ e^{-\left(\frac{11}{RT}\right)}\ C_{H_2} \\
fR_2 &= 10^{10}\ T^{0.734}\ e^{-\left(\frac{1.43}{RT}\right)}\ C_{OH} \\
rR_2 &= 3.68 \times 10^{8}\ T^{1.139}\ e^{-\left(\frac{17.1}{RT}\right)}\ C_{H_2O} \\
fR_3 &= 2 \times 10^{13}\ C_H \\
fR_4 &= 8 \times 10^{7}\ T^{1.56}\ e^{-\left(\frac{3.8}{RT}\right)}\ C_{C_2H_2} \\
fR_5 &= 2.2 \times 10^{12}\ e^{-\left(\frac{7.5}{RT}\right)}\ C_{O_2} \\
fR_6 &= 0.13\ C_{OH}
\end{aligned}
$$

$$
\begin{aligned}
\text{backward sum} &= rR1 + rR2 + fR3 + fR4 + fR5 \\
\text{forward sum} &= fR1 + fR2 \\
\text{Ratio fb} &= \frac{\text{forward sum}}{\text{backward sum}} \\
\text{sites} &= \pi\chi \left(\frac{6m_1}{\pi\rho_s}\right)^{2/3} \\
\text{eff sites} &= \alpha \times sites
\end{aligned}
$$

The parameter α is defined as:

$$
\begin{aligned}
\alpha &= \tanh(a/\log(\mu_1) + b) \\
a &= 12.65 - 5.63 \times 10^{-3}\ T \\
b &= -1.38 + 6.80 \times 10^{-4}\ T \\
\mu_1 &= \sum_{i=32}^{i_{max}} (N_i\ i)\ / \sum_{i=32}^{i_{max}} N_i
\end{aligned}
$$

χ is the estimated total surface carbon density / cm^2.

C Nomenclature

Table 4: *Nomenclature.*

Symbol	Expansion of Symbol	Value	Units
N_A	Avogadro Number	6.0243×10^{23}	mole^{-1}
k_B	Boltzmann constant	1.3807×10^{-16}	JK^{-1}
m_c, m_1	Mass of a carbon atom	12	amu
m_{OH}	Mass of a OH molecule	17	amu
d_1	Size of the benzene ring	0.242	nm
d_{PAH}	Diameter of a Pyrene molecule	0.79	nm
ρ_s	Density of soot	1.8	g cm^{-3}
C_{PAH}	Concentration of Pyrene		mol cm^{-3}
χ	Nominal number of sites	2.3×10^{15}	cm^{-2}
Kn_1	Knudsen number calculated for d_1		

References

[1] D. J. Aldous. Deterministic and stochastic models for coalescence (aggregation, coagulation): a review of the mean-field theory for probabilists. *BERNOULLI*, 5:3–48, 1999.

[2] J. Appel, H. Bockhorn, and M. Frenklach. Kinetic modeling of soot formation with detailed chemistry and physics: Laminar premixed flames of C_2 hydrocarbons. *Combustion and Flame*, 121:122–136, 2000.

[3] J. Appel, H. Bockhorn, and M. Wulkow. A detailed numerical study of the evolution of soot particle size distributions in laminar premixed flames. *Chemosphere*, 42:635–645, 2001.

[4] M. Balthasar and M. Kraft. A stochastic approach to calculate the particle size distribution function of soot particles in laminar premixed flame. *Combustion and Flame*, 133:289–298, 2003.

[5] H. Bockhorn. *Soot formation in Combustion: Mechanisms and Models*. Spreinger-Verlag, 1994.

[6] A. Eibeck and W. Wagner. Approximate solution of the coagulation-fragmentation equation by stochastic particle systems. *Stochastic Anal. Appl.*, 18:921–948, 2000.

[7] A. Eibeck and W. Wagner. An efficient stochastic algorithm for studying coagulation dynamics and gelation phenomena. *SIAM Journal of Sci. Comput.*, 22:802–821, 2000.

[8] A. Eibeck and W. Wagner. Stochastic interacting particle systems and nonlinear kinetic equations. *Ann. Appl. Probab.*, 13:845–889, 2003.

[9] George S Fishman. *Monte Carlo: Concepts, Algorithms and Applications*. Springer-Verlag, 1996.

[10] M. Frenklach. Soot formation codes. Technical report, http://www.me.berkeley.edu/soot/codes/codes.html, 1995.

[11] M. Frenklach. On surface growth mechanism of soot particles. *Proc. Combust. Inst.*, 26:2285–2293, 1996.

[12] M. Frenklach. Method of moments with interpolative closure. *Chemical Engineering Science*, 57:2229–2239, 2002.

[13] M. Frenklach and S. J. Harris. Aerosol dynamics modeling using the method of moments. *Journal of Colloid Interface Science*, 118:252–262, 1986.

[14] M. Frenklach and H. Wang. *Detailed Mechanism and Modeling of Soot Particle Formation*, pages 165–192. Springer-Verlag, 1994.

[15] A. G. Gaydon and H. G. Wolfhard. *Flames – Their structure, radiation and temperature*. Chapman and Hall Ltd., 1970.

[16] F. Gelbard and J. H. Seinfeld. Simulation of multicomponent aerosol dynamics. *Journal of Colloid Interface Science*, 78:485–501, 1980.

[17] D. T. Gillespie. An exact method for numerically simulating the stochastic coalescence process in a cloud. *Journal of Atmospheric Science*, 32:1977–1989, 1975.

[18] M. Goodson and M. Kraft. An efficient stochastic algorithm for simulating nano-particle dynamics. *Journal of Computational Physics*, 183:210–232, 2002.

[19] J. P. Hessler, S. Seifert, and R. E. Winans. Spatially resolved small-angle x-ray scattering studies of soot inception and growth. *Proc. Combust. Inst.*, 29:2743–2748, 2002.

[20] D. D. Huang, J. H. Seinfelf, and K. Okuyama. Image potential between a charged particle and uncharged particle in aerosol coagulation–enhancement in all size regimes and interplay with van der waals forces. *Journal of Colloid and Interface Science*, 141:191–198, 1991.

[21] A. Kazakov and M. Frenklach. Dynamic modeling of soot particle coagulation and aggregation: Implementation with method of moments and application to high- pressure laminar premixed flames. *Combustion and Flame*, 114:484–501, 1998.

[22] A. Kazakov, H. Wang, and M. Frenklach. Detailed modeling of soot formation in laminar premixed ethylene flames at a pressure of 10 bar. *Combustion and Flame*, 100:111–120, 1995.

[23] J. Kee, K. Grcar, M. D. Smooke, and J. A. Miller. Premix: A FORTRAN program for modelling steady laminar one-dimensional premixed flames. Technical report, SANDIA National Laboratories: SAND85-8240, 1985.

[24] I. M. Kennedy. Models of soot formation and oxidation. *Prog. Energy Combustion Science*, 23:95–132, 1997.

[25] F. Mauss, B. Trilken, H. Breitbach, and N. Peters. *Soot Formation in Combustion: Mechanisms and Models*, pages 325–349. Springer-Verlag, 1994.

[26] S. E. Pratsinis. Simultaneous nucleation, condensation and coagulation in aerosol reactors. *Journal of Colloid and Interface Science*, 124:416–427, 1988.

[27] K. Radhakrishnana and A. C. Hindmarsh. Description and use of LSODE, the livermore solver for ordinary differential equations. Technical report, LLNL Report, 1994.

[28] K. K. Sabelfeld, S. V. Rogasinsky, A. A. Kolodko, and A. I. Levykin. Stochastic algorithms for solving smoluchovsky coagulation equation and applications to aerosol growth simulation. *Monte Carlo Methods and Appl.*, 2:41–87, 1996.

[29] J. Singh, M. Balthasar, M. Kraft, and W. Wagner. Stochastic modelling of soot particle size and age distributions in laminar premixed flames. *Proc. Combust. Inst.*, 30:in–print, 2004.

[30] M. D. Smooke, R. J. Hall, M. B. Colket, J. Fielding, M. B. Long, C. S. McEnally, and L. D. Pfefferle. Investigation of the transtion from lightly sooting towards heavily sooting co-flow ethylene diffusion flames. *Combustion Theory and Modelling*, 8:593–606, 2004.

[31] M. von Smoluchowski. Drei Vorträge über Diffusion, Brownsche Molekularbewegung und Koagulation von Kolloidteilchen. *Phys. Z.*, 92:129, 1917.

[32] H. Wang and M. Frenklach. A detailed kinetic modeling study of aromatics formation in laminar premixed acetylene and ethylene flames. *Combustion and Flame*, 110:173–221, 1997.

[33] H. Wang, B. Zhao, B. Wyslouzil, and K. Streletzky. Small-angle neutron scattering of soot formed in laminar premixed ethylene flames. *Proc. Combust. Inst.*, 29:2749–2758, 2002.

[34] F. Xu, P. B. Sunderland, and G. M. Faeth. Soot formation in laminar premixed ethylene/air flames at atmospheric pressure. *Combustion and Flame*, 108:471–493, 1997.

[35] B. Zhao, Z. Yang, M. V. Johnston, H. Wang, A. S. Wexler, M. Balthasar, and M. Kraft. Measurement and numerical simulation of soot particle size distribution function in a laminar premixed ethylene-oxygen-argon flame. *Combustion and Flame*, 133:173–188, 2003.

[36] B. Zhao, Z. Yang, Z. Li, V. Johnston, and H. Wang. Particle size distribution function of incipient soot in laminar premixed ethylene flames: Effect of flame temperature. *Proc. Combust. Inst.*, 30:in–print, 2004.